Catalysis Science & Technology

Ethylene oligomerization into linear olefins over cobalt oxide on carbon catalyst

Journal:	*Catalysis Science & Technology*
Manuscript ID	CY-ART-02-2021-000207.R2
Article Type:	Paper
Date Submitted by the Author:	08-Apr-2021
Complete List of Authors:	Jonathan, Alvin; University of Wisconsin, Chemical and Biological Engineering Eagan, Nathaniel; Tufts University, Bruns, David; University of Wisconsin, Chemical and Biological Engineering Stahl, Shannon; University of Wisconsin-Madison, Department of Chemistry Lanci, Michael; ExxonMobil Research and Engineering Company Annandale Dumesic, James; University of Wisconsin Madison, Chemical and Biological Engineering Huber, George; University of Wisconsin, Chemical and Biological Engineering

ARTICLE

Ethylene oligomerization into linear olefins over cobalt oxide on carbon catalyst

Received 00th January 20xx,
Accepted 00th January 20xx

DOI: 10.1039/x0xx00000x

Alvin Jonathan,[a] Nathaniel M. Eagan,[a] David L. Bruns,[b] Shannon S. Stahl,[b] Michael P. Lanci,[c] James A. Dumesic,[a] and George W. Huber*[a]

Here, we show that C_4-C_{12} linear olefins, including linear alpha olefins, can be selectively produced from ethylene over a stable cobalt oxide on carbon catalyst. Both bulk and surface cobalt phases are CoO when the catalyst is stable, suggesting CoO is the stable cobalt phase for oligomerization. During the reaction, polyethylene forms in the catalyst pores which influences the product selectivity. The catalyst is more stable at higher temperatures (~ 200 °C) likely due to reduction of Co_3O_4 to CoO while rapid deactivation is observed at lower temperatures (e.g., 80-140 °C). The product selectivity can be fit to two different Schulz Flory distributions, one from C_4 to C_{10} olefins and one above C_{10} olefins, suggesting that transport restrictions influence product selectivity. At 48.3% conversion, product linearities up to C_{12} olefins are above 90%, making it the most selective heterogeneous catalyst to linear olefins to date in the absence of activators and/or solvents.

Introduction

The advent of hydraulic fracturing technologies and the discovery of additional natural gas sources have led to considerable increases in natural gas production since 2006.[1, 2] Steam cracking of natural gas produces light olefins including ethylene, one of the most manufactured commodity chemicals produced today.[3, 4] Ethylene can also be synthesized from dehydration of ethanol which is currently the most widely produced biofuel in the world.[5-7] Light C_2-C_4 olefins are important feedstocks in the production of linear alpha olefins (LAOs) for use in polyethylene comonomers (C_4 - C_8), plasticizers (C_6 - C_{10}), lubricants (C_{10} - C_{12}), and detergents (C_{10} - C_{16}).[8, 9] Higher linear olefins (C_{10}-C_{22}) are also valuable as they can be used as precursors for diesel fuels.[3] Current industrial processes for LAO synthesis involve the oligomerization of light olefins, often with homogeneous catalysts.[10-13] Olefin oligomerization has also been classically carried out over solid acids, though this typically produces highly branched products resulting from the underlying carbocation mechanisms.[3, 14, 15] Various attempts have been made to adapt the former technology to fully heterogeneous systems, most commonly by supporting nickel on aluminosilicates or metal organic frameworks (MOFs).[11, 12, 16-23] To date, these strategies have only obtained <60% selectivity to C_{8+} linear products at low conversions (e.g., <20%), with decreased linear product selectivity at higher conversion.[22]

Heterogeneous carbon-supported cobalt catalysts, on the other hand, have been reported to yield high selectivities to linear olefins.[24-31] Schultz et al. demonstrated that dimerization of propylene over a doubly ammoniated cobalt oxide on carbon catalyst (CoO_x/N-C) in a batch reactor at 85 °C yielded 52% selectivity to linear hexenes.[24] This catalyst was prepared by treating the activated carbon in a solution containing NH_4OH, followed by cobalt impregnation, and then a second treatment with NH_4OH. Schultz et al. also reported that dimerization of 1-butene and 1-hexene with this catalyst at 150 °C yielded 65% and 83% selectivities to linear dimers, respectively.[25] However, no catalyst stability study as a function of reaction time was reported in those reactions. Recently, Xu et al. demonstrated that ethylene oligomerization over a doubly ammoniated cobalt oxide on carbon catalyst (CoO_x/N-C) at 80 °C in a continuous flow reactor yielded octenes with 77.6% linearity but only 5.2% 1-octene at 20% conversion.[28] Xu et al. claimed that the addition of Cr to the doubly ammoniated cobalt oxide on carbon catalyst (Cr-CoO_x/N-C) improves the activity and stability of the catalyst.[31] However, these experiments were performed in a reaction condition where the catalyst deactivated losing of over 30% of the catalyst activity in a 12 h period. As we will show in this paper, the hypotheses of implementing ammonia and Cr to the catalyst to improve the activity or stability of the catalyst need to be tested in a regime where the catalyst is stable to prove their validity.

Kiani et al. investigated ethylene oligomerization over both cobalt on carbon and ammoniated cobalt on carbon catalysts at the reaction temperature of 80 °C. They performed *in-situ* DRIFTS, *in-situ* Raman, and *in-situ* UV-Vis to try and elucidate the nature of the active site of these catalysts.[32] Kiani et al. showed that the rate of 1-butene formation with both cobalt on carbon and ammoniated cobalt on carbon catalysts decreased by approximately 80% in an 8 h period at 80 °C. Both catalysts had similar activity for ethylene conversion and deactivation rates at 80 °C. Kiani et al. proposed that the active site is the immobilized pseudo-tetrahedral $[Co(NH_3)_x]^{2+}$,

[a] Department of Chemical and Biological Engineering, University of Wisconsin-Madison, Madison, WI, 53706, USA.
[b] Department of Chemistry, University of Wisconsin-Madison, Madison, WI, 53706, USA.
[c] ExxonMobil Research and Engineering, Annandale, NJ, 08801, USA.
† Footnotes relating to the title and/or authors should appear here.
Electronic Supplementary Information (ESI) available: [details of any supplementary information available should be included here]. See DOI: 10.1039/x0xx00000x

which was unfortunately not present in the cobalt on carbon catalyst (from the absence of the νNH wavenumber at 3325 cm^{-1} in their *in-situ* DRIFTS spectra).[32] Several fundamental questions need to be elucidated about these cobalt on carbon catalysts including how to reduce the rate of deactivation and what the active site is. It would also be desirable to be able to tune the product selectivity to linear alpha olefins (LAOs) instead of linear internal olefins as well as the selectivity to larger olefins (e.g., C_{8+}) while maintaining high product linearity. In this paper, we elucidate the reactions, the nature of the active site, the causes of catalyst deactivation, and how to tune the product selectivity for ethylene oligomerization over a carbon-supported cobalt catalyst.

Experimental

Catalyst synthesis

High-temperature-treated carbon (HTTC) was prepared by heating sieved activated carbon (Norit Darco MRX m-2278, 250-600 μm particle size, 600-800 $m^2\ g^{-1}$ BET surface area) at 900 °C for 2 h under 100 cm^3 (STP) min^{-1} of He at 10 °C min^{-1} ramp rate. The carbon support used in this paper is the same carbon used by Xu et al., Zhao et al., and Chada et al. (Norit Darco MRX m-1721), except with a different batch.[27-31] This is a different carbon support used by Schultz et al. (Pittsburgh Coke) and Kiani et al. (Alfa Aesar).[24-26, 32] After being cooled to room temperature, 2.0 g of the HTTC was impregnated with a solution composed of 1.89 g of $Co(NO_3)_2{\cdot}6H_2O$ (Sigma Aldrich) and 1.22 g of deionized (DI) water while exposed to air to obtain a Co loading of approximately 12 wt%. This loading was chosen for comparison to results obtained previously by Xu et al.[28, 31] The catalyst was dried overnight on a hotplate at 120 °C.

Continuous flow reactions

The ethylene oligomerization experiments were performed in 30 cm in length (1 ft) downflow fixed bed reactors with 1.27 cm (½ in) OD tubing for the reactions at 33.2% and 48.3% conversions, and 0.64 cm (¼ in) OD tubing for all other reactions. A diagram of this system is provided in Fig. S1. Both ethylene and argon flow rates were varied from 20 to 40 cm^3 (STP) min^{-1} while the amount of catalyst was varied from 0.5 to 13.0 g. The contact time for each experiment is defined as the ratio of the mass of catalyst to the inlet mass flow rate of ethylene (h $g_{cat}\ g_{ethylene}^{-1}$). Prior to the experiment, the catalyst was pretreated in the reactor at 230 °C (1 °C min^{-1} ramp rate) in 100 cm^3 (STP) min^{-1} of Ar for 2 h. The catalyst was cooled to room temperature, pressurized to 32 bar (450 psig) using a back-pressure regulator (Equilibar), and heated to the desired reaction temperature at 5 °C min^{-1} ramp rate under Ar, followed by a switch in feed. Each reaction was performed with a 50:50 mixture (by volume) of ethylene and argon. After the regulator, the product stream was directed to a 120 mL glass tube submerged in an ice bath to condense out heavier species. The vapor fraction was analyzed by an online gas chromatograph equipped with a flame ionization detector (GC-FID, Shimadzu) approximately every 45 minutes. The liquid product was washed with 10 g of heptane to ensure full collection and analyzed by a two-dimensional gas chromatograph equipped with a flame ionization detector (2D-GC-FID, Agilent) every 3 h. During liquid product collection, the reactor effluent was temporarily directed to a secondary condenser before a new condenser was installed. The details of the GC-FID and the 2D-GC-FID are described elsewhere, except the hold time for the GC-FID was changed to 16 min at 250 °C and the liner for the 2D-GC-FID was not packed with a Pd/C catalyst.[30]

Product quantification

The online GC-FID detected C_2-C_{10} species while the 2D-GC-FID detected C_2-C_{24} species. The online GC-FID was calibrated using a Scotty gas standard (a mixture of 0.1 mol% of each C_2-C_6 LAO and 99.5 mol% of He). For species heavier than C_6, a linear correlation of the inverse calibration constant with the carbon number was approximated, described in detail in the supplementary information. For the liquid product quantification, nonane was used as an internal standard, and the quantification was based on the effective carbon number approximation. The C_4 isomer distribution was determined using the online GC-FID while the isomer distributions of heavier species were analyzed by the 2D-GC-FID. LAO standards up to C_{24} and linear internal olefins standards up to C_8 were used to determine retention times. Representative 2D-GC-FID chromatograms for the overall products and the C_8 olefin species are shown in Fig. S2a and b, respectively. For species heavier than C_8, GC peaks with retention times later than the corresponding LAOs were assumed to be linear internal olefin based on the trends observed with the C_4, C_6, and C_8 olefins. In all cases, GC peaks with retention times earlier than the corresponding LAOs were assumed to be branched olefins. Isomer distributions of species heavier than C_{12} were not analyzed due to extensive GC peak overlap. Oxygenated products were not observed.

Data points before 6 h for experiments with ¼ in tubing and before 48 h for experiments with ½ in tubing were not included due to system transients. Carbon balances were above 97% for all reactions below 30% conversion, above 94% at 33.2% conversion, and above 91% at 48.3% conversion. Because transients have a particularly noticeable impact on isomer distributions, the product selectivity, linearity, and LAO isomer distribution for experiments with ¼ in tubing and ½ in tubing were calculated from the average of 12 to 24 h and 48 to 96 h data points, respectively. Error bars were calculated from the standard deviations of these data points.

Various parameters are defined as follows:

$$\text{Ethylene conversion (C\%)} = \frac{\sum_{i=4}^{n}(i \times F_{C_{i,\text{out}}})}{2 \times F_{C_{2,\text{in}}}} \times 100$$

$$\text{LAO isomer distribution of } C_i \text{ (C\%)} = \frac{F_{C_{i,\text{linear alpha,out}}}}{F_{C_{i,\text{out}}}} \times 100$$

$$\text{Product linearity of } C_i \text{ (C\%)} = \frac{F_{C_{i,\text{linear alpha,out}}} + F_{C_{i,\text{linear internal,out}}}}{F_{C_{i,\text{out}}}} \times 100$$

$$\text{Product selectivity of } C_i \text{ (C\%)} = \frac{i \times F_{C_{i,\text{out}}}}{\sum_{i=4}^{n}(i \times F_{C_{i,\text{out}}})} \times 100$$

$$\text{Ethylene consumption rate } (\text{mol}_{\text{ethylene}}\ g_{\text{cat}}^{-1}\ h^{-1}) = \frac{F_{C_{2,\text{in}}} \times \text{conversion}}{\text{mass of catalyst}}$$

$$\text{Carbon balance (C\%)} = \frac{\sum_{i=2}^{n}(i \times F_{C_{i,\text{out}}})}{2 \times F_{C_{2,\text{in}}}} \times 100$$

Here $\boldsymbol{F}$ is the molar flow rate in mol h^{-1} and $\mathbf{C}_{\boldsymbol{i}}$ represents all olefins of a specific structure (linear, linear alpha, or total) containing $\boldsymbol{i}$ carbon atoms.

Soxhlet extraction procedure

In a nitrogen-filled glovebox, the spent catalyst was removed from the sealed reactor tube and placed into a tared 24 mL scintillation vial. A portion of the spent catalyst was placed into a tared oven-dried cellulose thimble, on top of which was placed glass wool (to prevent the catalyst from escaping due to static electricity). The thimble was inserted into a Soxhlet extractor and then attached to a 250 mL round bottom flask with 100 mL of anhydrous toluene and a reflux condenser capped with a ground glass stopper. All ground glass joints were lightly greased with Apiezon H grease. The sealed Soxhlet assembly was removed from the glovebox and moved to a Schlenk line, placed under a positive pressure of N_2, and refluxed in an oil bath for 24 h. After 24 h, the round bottom flask replaced with a 25 mL Schlenk flask under a counterflow of N_2. Residual toluene in the Soxhlet assembly was removed *in vacuo* on the Schlenk line before being returned to the glovebox. The hot toluene extract was poured into 500 mL of acetone causing polyethylene to precipitate from solution. The precipitate was collected in a ground glass frit and washed several times with pentane to remove residual waxy pentane-soluble products. Before being transferred to a tared 24 mL scintillation vial, the precipitate was dried under vacuum to remove residual solvent. The filtrate was reduced on a rotary evaporator, and the remaining waxy residue was transferred to a tared 24 mL scintillation vial and dried under vacuum line to remove residual solvent.

X-ray diffraction (XRD) procedure

Powder XRD experiments were performed using a Rigaku Rapid II diffractometer with a Mo K_α source at 50 kV and 50 mA with the 2θ range of 2 to 45 ° and 30 min exposure time. For the XRD experiments without exposure to air, the catalysts were packed in glass capillaries with one end sealed with glass and the other end sealed by vacuum grease (Apiezon H vacuum grease) inside the glove box. This technique was applied to a highly pyrophoric material (diethylzinc) which did not react after three days outside of the glovebox, thus negligible oxygen entered the capillaries once exposed to air. These catalysts were transferred from the reactor to the glovebox either after pretreatment in argon at 230 °C for 2 h (fresh catalysts) or after reaction (spent catalysts) with both reactor tube ends sealed. For the experiments with exposure to air, the catalysts were packed inside a polyimide tube (American Durafilm) with both ends sealed with a clay. XRD experiments of the spent catalysts were performed prior to Soxhlet extractions. The XRD patterns of standards (e.g., carbon (graphite), polyethylene, and cobalt phases) were obtained from JADE 9 software. The baseline of each XRD pattern was corrected using JADE 9 software. The XRD detection limit of supported nanoparticles is typically 2-2.5 nm.[33]

X-ray photoelectron spectroscopy (XPS) procedure

XPS experiments were performed using a K-alpha spectrometer (Thermo Scientific) with a K_α X-ray source. All fresh and spent catalysts were packed into a vessel (Transfer Vessel K-Alpha) and sealed under vacuum inside a glovebox. These catalysts were analyzed without exposure to air. The fresh catalyst was pretreated in argon at 230 °C for 2 h before being transferred to the glovebox. The spent catalysts were treated with Soxhlet extractions without exposure to air to remove the liquid hydrocarbons in order to reach the 10^{-7} mbar vacuum requirement for XPS analyses. The Co_3O_4 and CoO standards (Sigma Aldrich, $\geq$ 99.5% trace metal basis) were analyzed with exposure to air. For the CoO standard, a monoatomic ion gun with 2000 eV was used with 90 s etch time to collect the spectrum. The collected CoO spectrum is consistent with the CoO spectrum from literature.[34] All samples were analyzed with the flood gun on. All binding energy (BE) values were calibrated to the BE of the C 1s peak for graphite at 284.5 eV. The Co 2p spectra were taken over 50 scans with 50 kV pass energy, 50 ms dwell time, and 0.1 eV step size. The C 1s spectra were taken over 20 scans with 50 kV pass energy, 50 ms dwell time, and 0.2 eV step size. The N 1s spectra were taken over 20 scans with 50 kV pass energy, 50 ms dwell time, and 0.2 eV step size. The baseline of each spectrum was corrected using a straight line. Intensities of all Co spectra were normalized to the Co spectrum from the spent 80 °C to have comparable intensities. The XPS detection limit is typically 0.1% to 1%.[35]

Attenuated total reflectance (ATR) procedure

Attenuated total reflectance FTIR (ATR-FTIR) spectra were collected on a Bruker Tensor 27 instrument with a Pike Technologies diamond ATR stage. Approximately 5 mg of precipitate collected in the Soxhlet extraction was used for each measurement. Spectra were collected at 4 cm^{-1} resolution between 4000-600 cm^{-1} with 16 scans and 16 background scans. High density polyethylene (HDPE, ExxonMobil, MW = 7845.30 Da) and low density polyethylene (LDPE, Dow 608A) were used as standards. The baselines of each spectrum were corrected using Origin 2015 software.

Thermogravimetric analysis (TGA) procedure

TGA experiments were performed using a Thermal Analysis Instruments Q500 system. For each measurement, approximately 10 mg of sample was heated at 10 °C min^{-1} under 50 cm^3 (STP) min^{-1} of N_2 to 800 °C.

N_2 physisorption procedure

N_2 physisorption experiments were performed using an ASAP 2020 (Micrometrics) at -196 °C. Approximately 200 mg of sample was used for each measurement. The sample was degassed for 6 h at 120 °C prior to the N_2 physisorption experiment. The Brunauer-Emmett-Teller (BET) surface areas were obtained from the N_2 physisorption data in the relative pressure (P/P_0) range of 0.06 to 0.24. The Barrett-Joyner-Halenda (BJH) pore size distributions (dV/dw where V is the pore volume and w is the pore width as a function of pore width) were obtained from the N_2 desorption isotherm.

Results and discussion

Ethylene oligomerization in continuous flow reactor

Supported cobalt oxide on carbon catalysts were synthesized using high-temperature-treated carbon (HTTC) heated at 900 °C in helium prior to incipient wetness impregnation of cobalt nitrate, described in detail in the experimental section. This high temperature treatment has been shown to remove sulfur impurities and oxygen

functional groups from activated carbon which could potentially affect the catalytic performance.[36] In addition, we neither incorporated ammonia treatment nor Cr to the catalysts to eliminate the potential contamination of the cobalt oxide on carbon catalysts (CoO_x/HTTC), especially when elucidating the active site. The plots of conversion and ethylene consumption rate of both CoO_x/HTTC and Cr-CoO_x/N-C at similar reaction conditions (i.e. 0.5 g of catalyst, ~40 cm^3 (STP) min^{-1} of ethylene, ~40 cm^3 (STP) min^{-1} of inert, 32 bar (450 psig) total pressure, and 80 °C reaction temperature) are shown in Fig. 1.[31] Fig. 1 shows that ethylene oligomerization reaction over CoO_x/HTTC is consistent both in terms of activity and stability with Cr-CoO_x/N-C obtained by Xu et al. at the reaction temperature of 80 °C.[31] For example, the present CoO_x/HTTC catalyst deactivated from 11.2% conversion at 6 h time on stream (TOS) to 7.3% conversion at 12 h TOS (35% activity loss) and subsequently to 3.5% conversion at 24 h TOS (70% activity loss). Xu et al. reported catalyst deactivation from 10% conversion at 6 h TOS to 6% conversion at 12 h TOS (40% activity loss). Data points before 6 h in this study are excluded due to system transients during startup. All ethylene oligomerization reactions in this study were performed with CoO_x/HTTC since this catalyst is simpler to study and analyze than the Cr-CoO_x/N-C.

We hypothesize that the CoO_x/HTTC catalyst initially deactivates before starting to stabilize, and this initial deactivation occurs faster at higher reaction temperature. To prove this hypothesis, ethylene oligomerization was carried out for 24 h periods at 80 °C and 200 °C with fresh catalysts, and at 80 °C with the catalyst previously used at 200 °C (for 24 h) to assess catalyst stability. Fig. 2a shows that the fresh catalyst at 80 °C loses 70% of its activity in 24 h. When the reaction was instead performed at 200 °C, the catalyst remained stable (Fig. 2a). After reaction at 200 °C, the catalyst can also be used

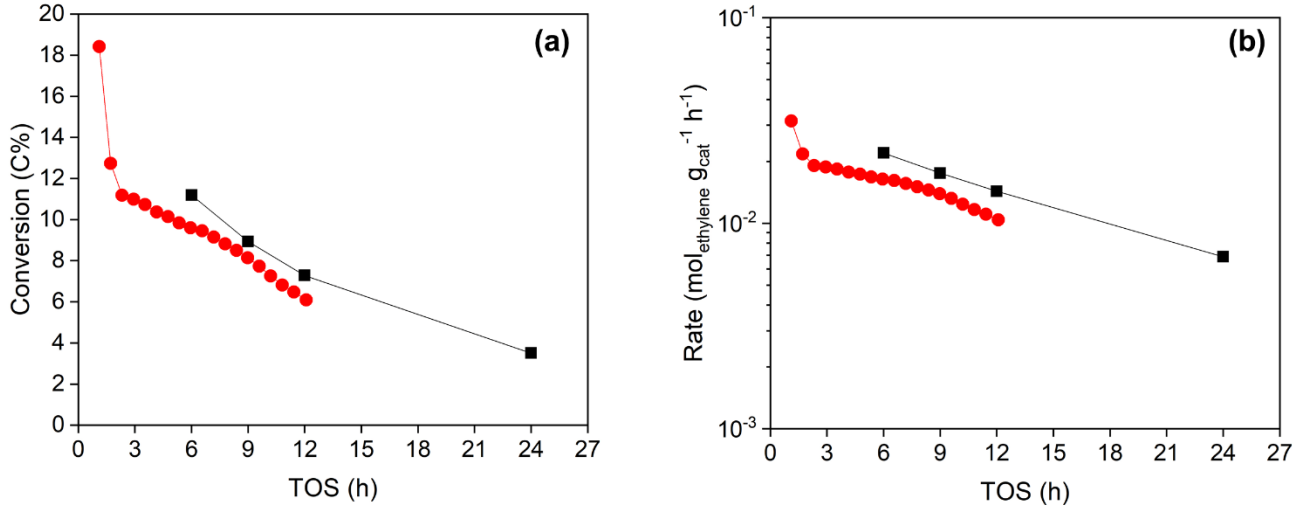

Fig. 1 Conversions and ethylene consumption rates of CoO_x/HTTC (black square) and Cr-CoO_x/N-C as reported by Xu et al. (red circle) for ethylene oligomerization at 80 °C.[31] (a) Ethylene conversions as a function of time on stream (TOS). (b) Ethylene consumption rates as a function of TOS. Reaction conditions in this study: 32 bar (450 psig) total pressure, 0.5 g of catalyst, 40 cm^3 (STP) min^{-1} of ethylene, 40 cm^3 (STP) min^{-1} of argon, and 0.18 h contact time. Reaction conditions from Xu et al.: 32 bar (450 psig) total pressure, 0.5 g of catalyst, 34.8 cm^3 (STP) min^{-1} of ethylene, and 45.4 cm^3 (STP) min^{-1} of helium.[31] Data points before 6 h in this study are excluded due to system transient.

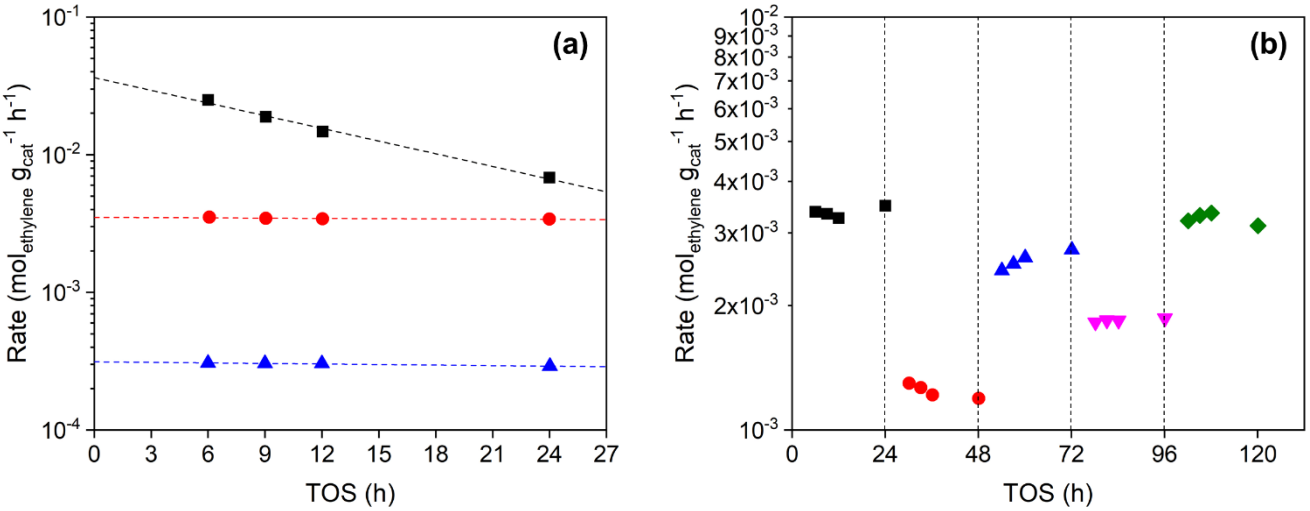

Fig. 2 Ethylene consumption rates versus time on stream (TOS) at different reaction temperatures. (a) Data points represent the following reaction temperatures: fresh 80 °C (black square), fresh 200 °C (red circle), and spent 80 °C after 200 °C (blue triangle). Dashed lines are added to guide the eye. Reaction conditions: 16 bar ethylene, 16 bar argon, 12 wt% CoO_x/HTTC, 0.18 h contact time for fresh 80 °C, and 1.45 h contact time for fresh 200 °C and spent 80 °C after 200 °C. (b) Data points represent the following reaction temperatures: first 200 °C (black square), 140 °C (red circle), 180 °C (blue triangle), 160 °C (magenta upside-down triangle), and last 200 °C (green diamond). Reaction conditions: 16 bar ethylene, 16 bar argon, 12 wt% CoO_x/HTTC, and 1.45 h contact time. Conversions were below 20% in all cases.

at 80 °C without deactivation albeit at a lower rate than with a fresh catalyst at 80 °C. This stability is further shown in Fig. 2b (rate versus TOS) and Fig. S3 (conversion versus TOS) for a series of temperatures with a single catalyst bed in the order 200-140-180-160-200 °C for 24 h each. The conversions from the first and final reactions at 200 °C were 13.7±0.4% and 13.2±0.4%, respectively, thus there is no statistically significant change in catalyst activity after 120 h of reaction. To further support this hypothesis, first order deactivation rate constants (k_d) were calculated for fresh catalysts at reaction temperatures of 80, 140, 160, 180, 200, and 220 °C for data collected over 24 h, shown in Fig. S4 (see the derivation of k_d in the supplementary information). The value of k_d decreased with increasing reaction temperature, consistent with the previous finding that operating at higher temperatures with fresh catalysts during a 24 h period yields more stable performance. A similar trend of increasing catalyst stability at higher reaction temperature was also observed in 1-butene dimerization over nickel zeolitic catalysts in the temperature range of 100-180 °C.[37] An apparent activation energy ($E_{a,app}$) of 25±1 kJ mol^{-1} was obtained using data where stable catalytic activities were observed—fresh catalyst reactions at 180, 200, and 220 °C as well the sequential reactions at 200-140-180-160-200 °C (Fig. S5).

The contact time for this catalyst was varied from 0.18 to 9.45 h g_{cat} $g_{ethylene}^{-1}$ at 200 °C and 32 bar (450 psig) total pressure to increase the conversion from 2.8 to 48.3% (Fig. S6) Fig. 3a shows the linear alpha olefin (LAO) isomer distributions of C_4, C_6, C_8, C_{10}, and C_{12} olefins as a function of conversion. C_{14+} olefin distributions are not shown due to substantial peak overlap in the GC. The LAO isomer distributions for all carbon numbers decreased with increasing conversion, likely resulting from more extensive isomerization with higher contact times. Fig. 3a shows that this catalyst is selective to LAOs among the C_4 to C_8 olefins at low conversions (e.g., <20%). At 14.0% conversion, the LAO isomer distributions of C_4, C_6, and C_8 olefins were 90.2%, 77.6%, and 69.1%, respectively. The product linearities of C_4 to C_{12} olefins, shown in Fig. S7, were all above 90% even at 48.3% conversion. To our knowledge this material is the most selective heterogeneous catalyst for ethylene oligomerization to linear olefins in the absence of activators and/or solvents.

Fig. 3b shows the product selectivities of C_4, C_6, C_8, C_{10}, and C_{12+} olefins as a function of conversion. The C_4 selectivity decreased from 59.8 to 50.6% as the conversion increased from 2.8 to 48.3%. This result demonstrates that the C_4 olefins can readsorb and further react with either ethylene or themselves to form larger olefins. Selectivities of C_6, C_8, and C_{10} olefins were relatively constant around 22%, 10%, and 5%, respectively, at these conversions. However, the selectivity of C_{12+} olefins increased the most from 4.1% to 10.9% with this increase in conversion.

Xu et al. reported that olefin oligomerization over CoO_x/N-C catalysts follows the Cossee-Arlman mechanism which results in a Schulz-Flory type distribution.[28] According to the Cossee-Arlman mechanism, a plot of $\log_{10}$(carbon selectivity/n) versus n, where n is the number of repeat units, will give a straight line with a slope corresponding to $\log_{10}(\alpha)$ where α is the chain growth probability. Additional details on the Schulz-Flory distribution are discussed in the supplementary information. A representative plot is shown in Fig. 4. We observed two different slopes for all reactions, one for C_4-C_{10} olefins and one for C_{10+} olefins. This trend was not observed in

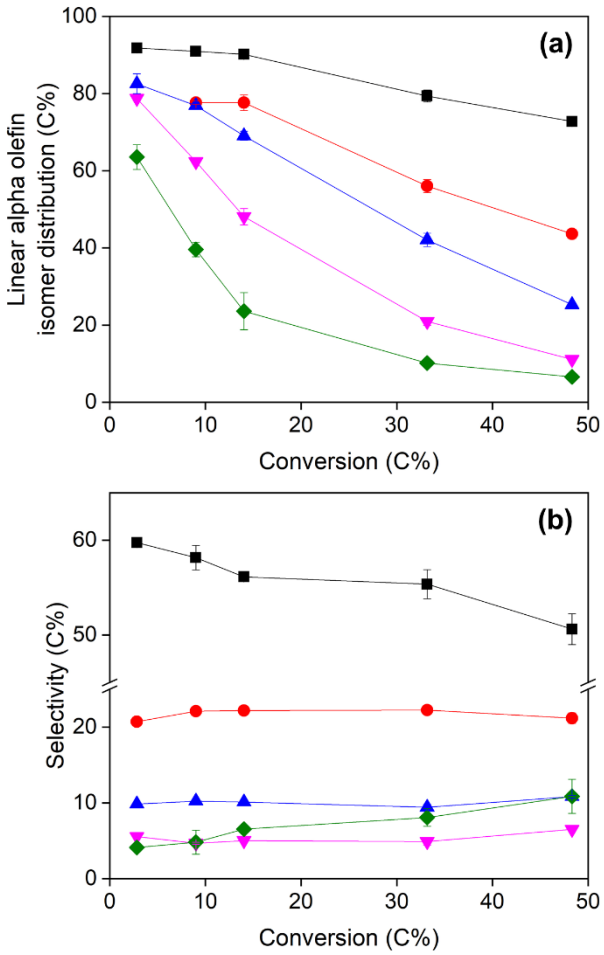

Fig. 3 Isomer distributions and product selectivities versus conversion. (a) Linear alpha olefin isomer distributions among C_4 (black square), C_6 (red circle), C_8 (blue triangle), C_{10} (magenta upside-down triangle), and C_{12} (green diamond) olefins versus conversion. (b), Selectivities of C_4 (black square), C_6 (red circle), C_8 (blue triangle), C_{10} (magenta upside-down triangle), and C_{12+} (green diamond) olefins versus conversion. Reaction conditions: 200 °C, 16 bar ethylene, 16 bar argon, 12 wt% CoO_x/HTTC, and 0.18 - 9.45 h contact time. Bounds represent standard deviations.

the prior work on ethylene oligomerization over CoO_x/N-C because the product distribution was only shown up to C_{12} olefins whereas our analysis goes up to C_{16} olefins.[28] Iglesia, Bell, and co-workers also observed similar behaviour of two different slopes in Fischer-Tropsch synthesis reactions.[38-40] Iglesia and co-workers proposed that the change in slope is due to intrapellet diffusion limitations for the larger olefins.[39] This result suggests that in the present study, C_{12+} olefins exhibit longer residence times inside the catalyst pores, increasing the probability that they react further before diffusing out. This behaviour could explain why the C_{12+} olefin selectivity increased the most with increasing conversion. Fig. S8 shows the α values (from C_4-C_{10} olefins and C_{10+} olefins) as a function of conversion. The value of α for C_4-C_{10} olefins was relatively constant around 0.33 while the value of α for C_{10+} olefins increased from 0.44 to 0.57 with increasing conversion from 2.8 to 48.3%.

We propose a possible reaction scheme shown in Fig. 5 for ethylene oligomerization over a heterogeneous cobalt on carbon catalyst. Ethylene is adsorbed onto the catalyst, after which ethylene

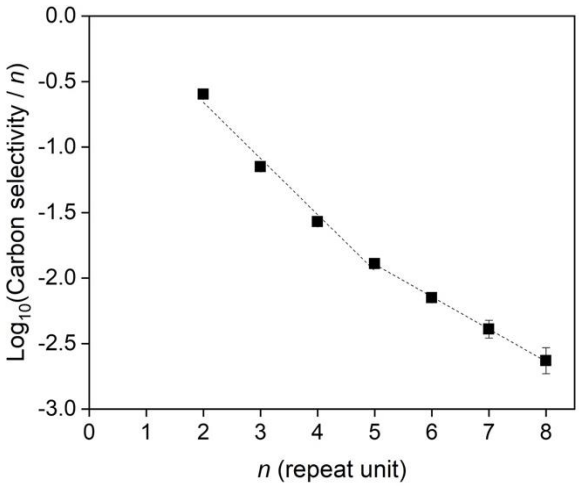

Fig. 4 A typical product distribution for ethylene oligomerization over CoO_x/HTTC as a function of repeat unit (*n*). Reaction conditions: 200 °C, 16 bar ethylene, 16 bar argon, 12 wt% CoO_x/HTTC, 9.45 h contact time, and 48.3% conversion.

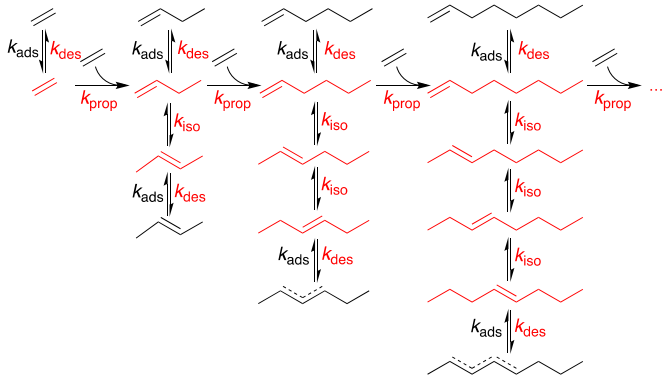

Fig. 5 Reaction scheme for ethylene oligomerization over a cobalt oxide on carbon catalyst. Higher olefins may also react with C_{4+} alkyl chains forming internal olefins (not depicted). Species and reactions on the catalyst surface are labelled with red color.

either desorbs or propagates with other ethylene molecules to extend the olefin chain length. The olefin chains continue to grow or desorb from the catalyst as LAOs. These olefins may also readsorb onto the catalyst after which isomerization may occur to yield linear internal olefins. This hypothesis is consistent with our observation that internal olefin selectivities increase with contact time, allowing each olefin more chances to readsorb and isomerize. Branched olefins are not shown in the reaction scheme as they represent less than 10% of the products. Coupling reactions between C_{4+} olefins to yield larger linear internal olefins may also occur and have only been omitted from this diagram for simplicity.[28]

Characterizations of fresh and spent catalysts

We investigated both the bulk and surface cobalt phases of the fresh catalyst after pretreatment in argon at 230 °C, the spent catalyst after a 24 h reaction at 80 °C, and the spent catalyst after a 24 h reaction at 200 °C. The X-ray diffraction (XRD) patterns of these catalysts were collected without exposure to air and are shown in Fig. 6a. Both the fresh and spent 80 °C catalysts showed clear Co_3O_4 reflections, consistent with the work by Xu et al.[28] The XRD pattern of the spent 200 °C catalyst, on the other hand, showed reflection characteristic of CoO, suggesting that the Co_3O_4 had been reduced during the reaction and furthermore that CoO is the more stable bulk phase during oligomerization. Peaks attributable to polyethylene were also observed in the spent 80 °C and spent 200 °C catalysts, suggesting the reaction produced polyethylene with relatively high crystallinity. XRD patterns of air-exposed fresh and spent catalysts from different reaction temperatures were also examined (Fig. S9), which similarly showed CoO being present in all stable catalysts.

X-ray photoelectron spectroscopy (XPS) measurements of the surface cobalt phase for the fresh, spent 80 °C, and spent 200 °C catalysts were collected without exposure to air. Using an air-free glovebox and Schlenk line techniques, the spent catalysts were initially washed with toluene in a Soxhlet extractor to remove volatile hydrocarbons to meet the vacuum requirements of the XPS instrument. The Co 2p XPS region of these three catalysts along with Co_3O_4 and CoO standards are shown in Fig. 6b. Co_3O_4 and CoO can be distinguished by comparing the satellite peaks in the Co 2p region.[34] Co_3O_4 has a satellite peak near 790 eV, while CoO has satellite peaks around 786 and 802 eV. All catalysts showed predominantly CoO features, although the spent 200 °C catalyst showed more prominent 786 and 802 eV features than did the fresh and spent 80 °C catalysts, suggesting that a higher fraction of its cobalt surface was in the CoO state. Metallic Co with a characteristic peak at 778 eV was not observed on any of these catalysts. Xu et al. reported that the distribution of Co_3O_4 and CoO according to XANES for CoO_x/N-C catalyst after pretreatment at 230 °C in helium without exposure to air was 72.5 and 27.5 wt%, respectively.[27] These results suggest that Co_3O_4 and/or CoO could be the active catalytic site(s) for oligomerization with different catalyst stability. It is unclear why the catalyst deactivated during a 24 h reaction at 80 °C whereas it was stable during a 24 h reaction at 200 °C when CoO was present on both catalysts. We hypothesize that the catalyst stability during the reaction at 200 °C could be related to the formation of bulk and surface CoO. We also investigated the N 1s XPS region of the fresh catalyst after pretreatment in argon at 230 °C without exposure to air to determine whether nitrogen was present in the catalyst before the oligomerization reaction. Fig. S10 shows that the N 1s XPS signal is within the noise level of the instrument, thus the active catalytic site of this catalyst is not related to nitrogen.

Thermogravimetric analysis (TGA) under N_2 was performed on the spent 80 °C and spent 200 °C catalysts before and after Soxhlet extractions to probe the presence of polyethylene and to determine whether the catalysts were free from oligomers after the extraction (Fig. S11). Before the Soxhlet extractions (Fig. S11a-b), both the spent 80 °C and spent 200 °C catalysts exhibited a peak near 430 °C, in agreement with the traces obtained by Zhao et al. for polyethylene TGA under N_2.[41] After the extractions, the TGA curves of both spent 80 °C and spent 200 °C catalysts (Fig. S11c-d) still contained oligomers and polyethylene. These hydrocarbons were likely formed inside the catalyst pores during the reaction and may have been too large to diffuse out during extraction.

N_2 physisorption experiments were performed on the fresh, spent 80 °C, and spent 200 °C catalysts to obtain BET surface areas (Table S1) and pore size distributions (Fig. S12). The spent catalysts were previously treated with Soxhlet extractions due to the vacuum requirements of the adsorption equipment. The BET surface areas of the spent 80 °C and spent 200 °C catalysts were 70 and 105 $m^2\ g^{-1}$, respectively, substantially lower than the BET surface area of the

fresh catalyst of 418 m^2 g^{-1}. The loss of BET surface area can be explained by the presence of remnant hydrocarbons including polyethylene which could not be fully removed with the extractions. The pore size distributions of these catalysts were similar, suggesting that polyethylene formation impacts all pores equally.

To provide further evidence for the presence of polyethylene, the hot toluene extracts from both spent catalysts were diluted with acetone to promote the precipitation of dissolved solids. The precipitate was collected by filtration and washed with pentane to remove pentane-soluble hydrocarbon fractions before being dried under vacuum. The resulting solids were analyzed by attenuated total reflectance FTIR (ATR-FTIR) along with high density (HDPE) and low density polyethylene (LDPE) standards, shown in Fig. 6c. All samples (spent 200 °C and spent 80 °C extracts along with the HDPE and LDPE standards) showed the same characteristic peaks near 719, 1462, 2848, and 2915 cm^{-1}, suggesting polyethylene was present in both spent catalysts. Schultz et al. also reported that the extract of the spent CoO_x/N-C catalyst after propylene dimerization had a molecular weight of 2000-3000 Da which they hypothesized to cause catalyst deactivation.[24]

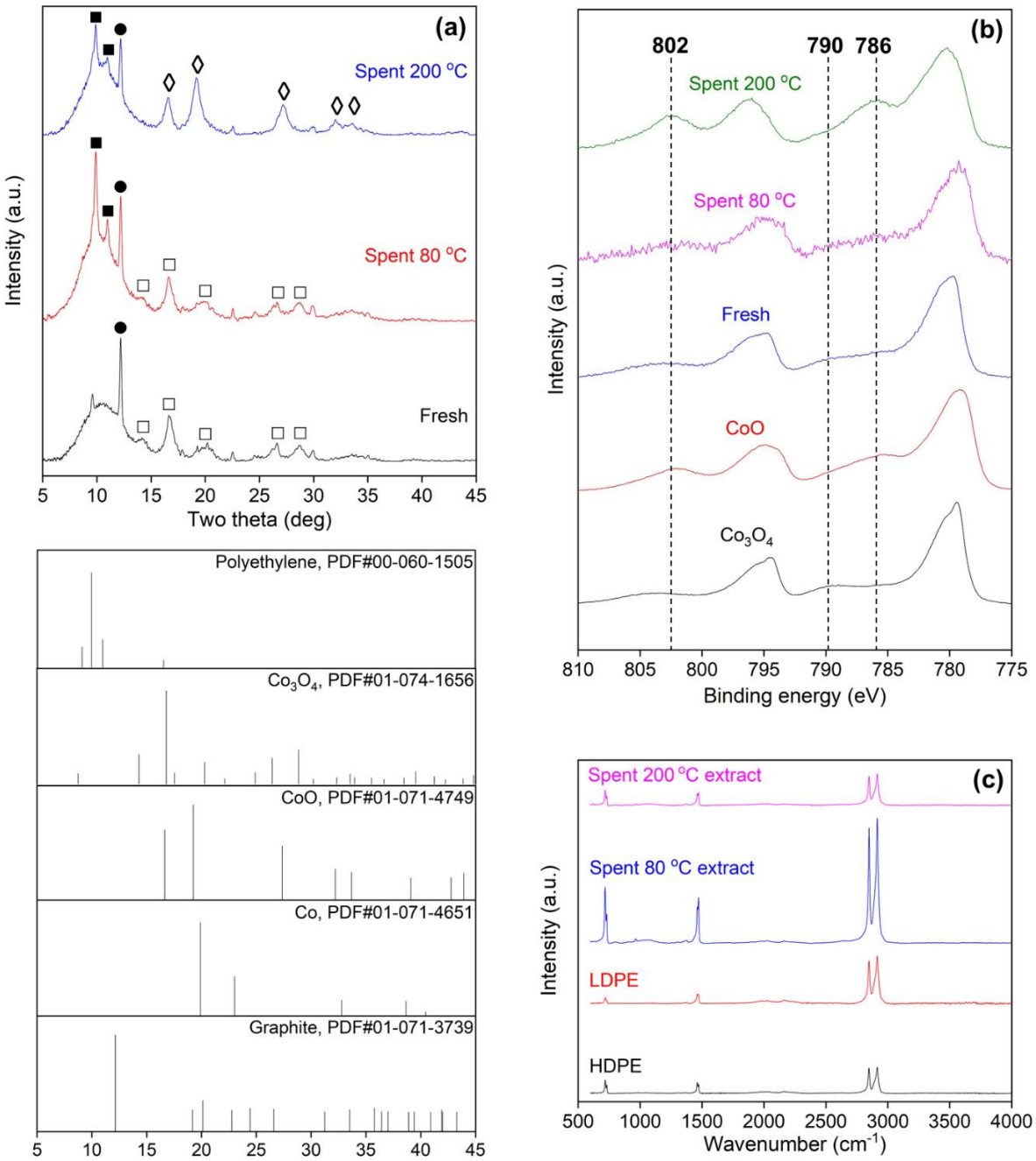

Fig. 6 XRD patterns and XPS spectra of fresh and spent catalysts as well as ATR spectra of the extracts from spent catalysts. (a) Mo-XRD of fresh catalyst after pretreatment in argon at 230 °C, spent catalyst after a 24 h reaction at 80 °C, and spent catalyst after a 24 h reaction at 200 °C before Soxhlet extractions. Characteristic peaks are carbon (graphite) - filled circle, polyethylene - filled square, Co_3O_4 - unfilled square, and CoO - unfilled diamond. (b) Co 2p XPS region of fresh catalyst after pretreatment in argon at 230 °C, spent catalyst after a 24 h reaction at 80 °C, and spent catalyst after a 24 h reaction at 200 °C after Soxhlet extractions along with Co_3O_4, and CoO standards. (c) ATR of polyethylene standards (HDPE and LDPE) and extracts from spent catalysts after 24 h reactions at 80 °C and 200 °C.

Conclusions

CoO_x/HTTC can selectively oligomerize ethylene into linear C_4-C_{12} olefins. The presence of CoO in the bulk and the surface cobalt phases suggests that this is the stable cobalt phase for oligomerization. At higher reaction temperatures (~ 200 °C) the catalyst is reduced from Co_3O_4 to the more stable CoO phase leading to improved catalyst stability. However, the presence of both Co_3O_4 and CoO in the fresh and spent catalysts after a 24 h reaction at 80 °C could suggest that both cobalt states are active for oligomerization. Polyethylene is formed in the catalyst pores during the reaction. The product distribution follows two different Schulz-Flory distributions with the first distribution from C_4 to C_{10} olefins and the second distribution above C_{10} olefins. This shift in product distribution indicates that transport restrictions, likely imposed by the oligomers and polyethylene in the pores, influence the product selectivity similar to chain growth during the Fischer-Tropsch Synthesis reaction. We propose a reaction scheme for this reaction, in which ethylene is adsorbed onto the catalyst, after which it either desorbs or propagates with other olefins. At lower conversion (<20%) high selectivity of C_4-C_8 linear alpha olefins (>60% LAO isomer distributions) is obtained while at higher conversion the selectivity to LAOs decreases due to isomerization and chain terminating internal olefin production. In short, these findings show that CoO_x/HTTC is a uniquely stable heterogeneous catalyst that produces highly linear (including linear alpha) olefin products from ethylene without requiring solvents or activators.

Conflicts of interest

There are no conflicts to declare

Acknowledgements

This work is supported by ExxonMobil. D. L. B. was supported by the NSF (CHE-1953926; SSS). The authors gratefully acknowledge use of facilities and instrumentation supported by NSF through the University of Wisconsin Materials Research Science and Engineering Center (DMR-1720415). The authors also thank Dr. Joseph P. Chada for useful discussions.

Notes and references

1. T. Ridha, Y. Li, E. Gençer, J. Siirola, J. Miller, F. Ribeiro and R. Agrawal, *Processes*, 2018, **6**, 139.
2. US Energy Information Administration. Annual energy outlook 2019 with projections to 2050. https://www.eia.gov/outlooks/aeo/pdf/aeo2019.pdf (Accessed February 2021).
3. N. M. Eagan, M. D. Kumbhalkar, J. S. Buchanan, J. A. Dumesic and G. W. Huber, *Nat. Rev. Chem.*, 2019, **3**, 223-249.
4. N. Rahimi and R. Karimzadeh, *Appl. Catal. A*, 2011, **398**, 1-17.
5. M. Balat and H. Balat, *Appl. Energy*, 2009, **86**, 2273-2282.
6. K. Kohse-Höinghaus, P. Oßwald, T. A. Cool, T. Kasper, N. Hansen, F. Qi, C. K. Westbrook and P. R. Westmoreland, *Angew. Chem. Int. Ed.*, 2010, **49**, 3572-3597.
7. G. Hochman and D. Zilberman, *Am. J. Agric. Econ.*, 2018, **100**, 570-584.
8. E. O. C. Greiner, M. Blagoev and Y. Yamaguchi, *Chemical Economics Handbook: Linear alpha-Olefins*, IHS Chemical, 2013.
9. G. R. Lappin, L. H. Nemec, J. D. Sauer and J. D. Wagner, *Kirk-Othmer Encyclopedia of Chemical Technology*, John Wiley & Sons, Inc., 2000.
10. C. P. Nicholas, *Appl. Catal. A*, 2017, **543**, 82-97.
11. R. Y. Brogaard and U. Olsbye, *ACS Catal.*, 2016, **6**, 1205-1214.
12. S. Moussa, P. Concepción, M. A. Arribas and A. Martínez, *ACS Catal.*, 2018, **8**, 3903-3912.
13. Z. Wang, G. A. Solan, W. Zhang and W.-H. Sun, *Coord. Chem. Rev.*, 2018, **363**, 92-108.
14. Y. T. Kim, J. P. Chada, Z. Xu, Y. J. Pagan-Torres, D. C. Rosenfeld, W. L. Winniford, E. Schmidt and G. W. Huber, *J. Catal.*, 2015, **323**, 33-44.
15. M. L. Sarazen, E. Doskocil and E. Iglesia, *J. Catal.*, 2016, **344**, 553-569.
16. M. A. Deimund, J. Labinger and M. E. Davis, *ACS Catal*, 2014, **4**, 4189-4195.
17. A. N. Mlinar, G. B. Baur, G. G. Bong and A. T. Bell, *J. Catal.*, 2012, **296**, 156-164.
18. I. Agirrezabal-Telleria and E. Iglesia, *J. Catal.*, 2017, **352**, 505-514.
19. E. D. Metzger, R. J. Comito, Z. Wu, G. Zhang, R. C. Dubey, W. Xu, J. T. Miller and M. Dincă, *ACS Sustain. Chem. Eng.*, 2019, **7**, 6654-6661.
20. A. Finiels, F. Fajula and V. Hulea, *Catal. Sci. Technol.*, 2014, **4**, 2412-2426.
21. R. Joshi, G. Zhang, J. T. Miller and R. Gounder, *ACS Catal.*, 2018, **8**, 11407-11422.
22. A. Ehrmaier, Y. Liu, S. Peitz, A. Jentys, Y.-H. Chin, M. Sanchez-Sanchez, R. Bermejo-Deval and J. A. Lercher, *ACS Catal.*, 2019, **9**, 315-324.
23. H. Olivier-Bourbigou, P. Breuil, L. Magna, T. Michel, M. F. Espada Pastor and D. Delcroix, *Chem. Rev.*, 2020, **120**, 7919-7983.
24. R. G. Schultz, J. Schuck and B. Wildi, *J. Catal.*, 1966, **6**, 385-396.
25. R. G. Schultz, R. M. Engelbrecht, R. N. Moore and L. T. Wolford, *J. Catal.*, 1966, **6**, 419-424.
26. R. G. Schultz, *J. Catal.*, 1967, **7**, 286-290.
27. Z. Xu, J. P. Chada, D. Zhao, C. A. Carrero, Y. T. Kim, D. C. Rosenfeld, J. L. Rogers, S. J. Rozeveld, I. Hermans and G. W. Huber, *ACS Catal.*, 2016, **6**, 3815–3825.
28. Z. Xu, D. Zhao, J. P. Chada, D. C. Rosenfeld, J. L. Rogers, I. Hermans and G. W. Huber, *J. Catal*, 2017, **354**, 213-222.
29. D. Zhao, Z. Xu, J. P. Chada, C. A. Carrero, D. C. Rosenfeld, J. L. Rogers, I. Hermans, and G. W. Huber, *ACS Catal.*, 2017**, 7**, 7479-7489.
30. J. P. Chada, Z. Xu, D. Zhao, R. B. Watson, M. Brammer, M. Bigi, D. C. Rosenfeld, I. Hermans and G. W. Huber, *Catal. Commun.,* 2018, **114**, 93-97.
31. Z. Xu, J. P. Chada, L. Xu, D. Zhao, D. C. Rosenfeld, J. L. Rogers, I. Hermans, M. Mavrikakis and G. W. Huber, *ACS Catal.*, 2018, **8**, 2488-2497.
32. D. Kiani and J. Baltrusaitis, *Catal. Today*, 2020, DOI: 10.1016/j.cattod.2020.04.062.
33. K. O'Connell and J. R. Regalbuto, *Catal. Lett.,* 2015, **145**, 777-783.
34. D. Gu, C.-J. Jia, C. Weidenthaler, H.-J. Bongard, B. Spliethoff, W. Schmidt and F. Schüth, *J. Am. Chem. Soc.*, 2015, **137**, 11407-11418.
35. A. G. Shard, *Surf. Interface Anal.*, 2014, **46**, 175-185.
36. P. E. Fanning and M. A. Vannice, *Carbon*, 1993, **31**, 721-730.
37. P. Beltrame, L. Forni, A. Talamini, and G. Zuretti, *Appl. Catal. A,* 1994**, 110**, 39-48.

38. E. Iglesia, *Appl. Catal. A*, 1997, **161**, 59-78.
39. E. Iglesia, S. C. Reyes, R. J. Madon and S. L. Soled, *Adv. Catal.*, 1993, **39**, 221-302.
40. R. A. Dictor and A. T. Bell, *J. Catal.*, 1986, **97**, 121-136.
41. D. Zhao, X. Wang, J. B. Miller and G. W. Huber, *ChemSusChem*, 2020, **13**, 1764-1774.